Laboratory Investigation (2021) 101:1098–1109
https://doi.org/10.1038/s41374-021-00600-x

TECHNICAL REPORT

Surface color spectrophotometry in a murine model of steatosis: an accurate technique with potential applicability in liver procurement

K. S. Kanamori[1] · M. G. Tarragó[1] · A. Jones[2] · E. H. Cheek[3] · G. M. Warner[1] · S. M. Jenkins[4] · D. Povero[5] · R. P. Graham[3] · T. Mounajjed[3] · M. F. Chedid[6] · B. D. Sabat[7] · M. S. Torbenson[3] · J. K. Heimbach[8] · E. N. Chini[1] · R. K. Moreira[3]

Received: 21 January 2021 / Revised: 5 March 2021 / Accepted: 5 March 2021 / Published online: 15 April 2021

Abstract

Steatosis is the most important prognostic histologic feature in the setting of liver procurement. The currently utilized diagnostic methods, including gross evaluation and frozen section examination, have important shortcomings. Novel techniques that offer advantages over the current tools could be of significant practical utility. The aim of this study is to evaluate the accuracy of surface color spectrophotometry in the quantitative assessment of steatosis in a murine model of fatty liver. C57BL/6 mice were divided into a control group receiving normal chow ($n = 19$), and two steatosis groups receiving high-fat diets for up to 20 weeks—mild steatosis ($n = 10$) and moderate-to-severe steatosis ($n = 19$). Mouse liver surfaces were scanned with a hand-held spectrophotometer (CM-600D; Konica-Minolta, Osaka, Japan). Spectral reflectance data and color space values (L*a*b*, XYZ, L*c*h*, RBG, and CMYK) were correlated with histopathologic steatosis evaluation by visual estimate, digital image analysis (DIA), as well as biochemical tissue triglyceride measurement. Spectral reflectance and most color space values were very strongly correlated with histologic assessment of total steatosis, with the best predictor being % reflectance at 700 nm ($r = 0.91$ [0.88–0.94] for visual assessment, $r = 0.92$ [0.88–0.95] for DIA of H&E slides, $r = 0.92$ [0.87–0.95] for DIA of oil-red-O stains, and $r = 0.78$ [0.63–0.87] for biochemical tissue triglyceride measurement, $p < 0.0001$ for all). Several spectrophotometric parameters were also independently predictive of large droplet steatosis. In conclusion, hepatic steatosis can accurately be assessed using a portable, commercially available hand-held spectrophotometer device. If similarly accurate in human livers, this technique could be utilized as a point-of-care tool for the quantitation of steatosis, which may be especially valuable in assessing livers during deceased donor organ procurement.

Introduction

Hepatic steatosis is the primary histopathologic abnormality of interest in assessing the suitability of liver allografts for possible transplantation, as the degree of fatty change in allografts represents a well-established risk factor for various adverse

These authors contributed equally: K. S. Kanamori, M. G. Tarragó

Supplementary information The online version contains supplementary material available at https://doi.org/10.1038/s41374-021-00600-x.

✉ R. K. Moreira
moreira.roger@mayo.edu

1 Signal Transduction and Molecular Nutrition Laboratory, Kogod Aging Center, Department of Anesthesiology and Perioperative Medicine, Mayo Clinic College of Medicine, Rochester, MN, USA

2 Clinical Pathology Associates, Austin, TX, USA

3 Department of Laboratory Medicine and Pathology, Mayo Clinic, Rochester, MN, USA

4 Division of Biomedical Statistics and Informatics, Mayo Clinic, Rochester, MN, USA

5 Department of Biochemistry and Molecular Biology, Mayo Clinic College of Medicine, Rochester, MN, USA

6 Liver and Pancreas Transplant and Hepatobiliary Surgery Unit, Hospital de Clinicas de Porto Alegre, Federal University of Rio Grande do Sul (UFRGS), Porto Alegre, Brazil

7 Faculdade de Ciências Médicas, Universidade de Pernambuco, Recife, Brazil

8 Division of Transplant Surgery, William J. von Liebig Transplant Center, Mayo Clinic, Rochester, MN, USA

outcomes, including preservation injury, primary nonfunction, and early allograft dysfunction [1, 2]. The risk for these adverse outcomes has been shown to correlate with the estimated grade of steatosis in donor livers, being the lowest in donor livers containing <30% large droplet macrovesicular steatosis and the highest in those showing over 60%.

While histopathologic semiquantitative analysis of hematoxylin and eosin (H&E) slides from formalin-fixed paraffin-embedded tissue (with or without the aid of "fat stains" such as oil-red-O [ORO] or Sudan IV) by a liver pathologist has been the standard for grading of steatosis, frozen section diagnosis represents an acceptable, albeit imperfect, surrogate method that depends on the timely processing of liver samples in the frozen section laboratory and on the immediate availability of a pathologist with expertise in this area.

In view of these challenges, we believe that the utilization of color sensing and analysis technology may represent a significantly more precise, objective, and reproducible way of characterizing the color of liver tissue and may lead to better correlation with various degrees of steatosis. Among several methods that could be used in this context, spectrophotometry (whereby beams of reflected or transmitted light are separated into their component wavelengths and the spectral reflectance of an object at each wavelength is measured) is generally regarded as the gold standard for color analysis and represents the most suitable technology to be utilized in this setting. Highly accurate devices are commercially available and are already widely utilized in industry (cosmetic dentistry, textile, paint, synthetic materials, food industry, among others) [3–5] and, to a more limited extent, in medical practice [6–11]. These devices are able to analyze the color of objects with a high degree of precision and reproducibility, regardless of shape, texture, consistency, and reflective properties, which are necessary attributes for the analysis of human tissue samples. In addition, hand-held models are available and could potentially be used as point-of-care diagnostic tools during procurement.

In this study, we utilized a hand-held, commercially available spectrophotometer device and analyzed light reflectance within the visual spectrum (400–700 nm) as well as its associated color coordinates in different color spaces, in an attempt to more objectively describe the spectrophotometric features of livers with various degrees of steatosis in a murine model of fatty liver disease. Findings were correlated with quantitative and semiquantitative histopathologic analysis, digital image analysis (DIA), and biochemical tissue lipid measurements.

Materials and methods

Steatosis induction

All protocols and procedures were approved by our hospital's Institutional Animal Care and Use Committee, and studies were conducted in adherence to the NIH Guide for the Care and Use of Laboratory Animals. We utilized male C57BL/6 mice obtained from Jackson Laboratories (Bar Harbor, MA), which were housed in standard cages at constant temperature and humidity, with 12-h light–dark cycles. Mice in the control group (S0) ($n = 19$) were maintained on a normal chow diet (PicoLab 5053 Rodent Diet 20; LabDiet) ad libitum. Mice in the mild steatosis (S1) ($n = 10$) and moderate-to-severe steatosis (S2–3) ($n = 19$) groups were maintained on D12492 (60-kcal% fat; Research Diets, Inc.), or high-fat diet (HFD), for 2–4 and 8–20 weeks, respectively. Mice were weighed weekly and immediately before tissue collection.

Tissue collection

Mice were euthanized at 23–30 weeks of age via isoflurane inhalation overdose. Immediately following abdominal incision, the portal vein was cannulated with a 23-G needle attached to a 5-ml syringe. Cold University of Wisconsin (UW) solution (ViaSpan) was used to flush the liver, with an initial infusion of 1–2 ml, followed by transection of the inferior vena cava for hepatic blood drainage. The infusion was continued, with light manual pressure, until the liver was uniformly flushed, using a minimum of 15 ml of UW solution for each liver. After hepatectomy and spectrophotometric measurements, liver tissue was weighed and samples were collected for histopathologic and biochemical analysis.

Spectrophotometric measurement and analysis

Color measurements were taken using a hand-held spectrophotometer (CM-600D; Konica-Minolta, Osaka, Japan) with an 8-mm target mask (Fig. 1). This spectrophotometer device emits "white" light (specifically, Commission on Illumination [CIE] Standard Illuminant D65) generated by a pulsed xenon lamp with UV cut filter and analyzes reflectance within the 400–700-nm wavelength range. After flushing with UW solution, the liver was excised, cleaned of surface blood, and placed directly over the 8-mm opening of the target mask, which was covered by a translucent, impermeable adhesive film (Tegaderm^{TM}) (Supplementary Fig. 1). The instrument was calibrated using a standard white calibration cap immediately before collecting data on every sample. Each liver was scanned twice (at the same site, left lateral lobe, due to limitations in the availability of relatively large and flat liver surfaces in mouse livers). Spectrophotometric data were subsequently processed using SpectraMagic NX Color Data Software Professional Edition CM-100w Ver. 2.8 (Konica-Minolta Sensing Americas, Inc.). Analyzed data included spectral reflectance graph (utilizing Specular Component Included mode, which

Fig. 1 Hand-held spectrophotometer. External appearance of the device.

encompasses both specular and diffuse reflection) and color spaces L*a*b*, L*c*h*, and XYZ. RGB and CMYK color system models were also calculated from L*a*b* values. Color coordinate numbers have the following ranges: L*, 0–100; a* and b*, −128 to 128; c*, 0–100; h*, 0–359.9; X, 0–96.42; Y, 0–100; Z, 0–82.52; and R, B and G, 0–255.

Histologic stains

Liver tissue samples were fixed in 10% neutral buffered formalin, embedded in paraffin, cut at 4-µm sections, and stained with H&E (for visual and digital analysis of steatosis) and Masson trichrome (for exclusion of fibrosis) stains. ORO stains (for digital analysis) were also performed using frozen liver tissue in optimal cutting temperature medium, sectioned at 10 µm.

Visual semiquantitative steatosis analysis

Slides were independently and blindly reviewed by three expert gastrointestinal/liver pathologists for classification of each liver into one of the following categories: no steatosis, mild steatosis (<30%), moderate steatosis (30–60%), and severe steatosis (>60%). In case of discrepant categorization by different pathologists, the final classification of a given case would be either by majority opinion (if two of three pathologists are in agreement) or by re-review of the case by the three pathologists for a consensus (if all three interpretations are different). One pathologist (RKM) assessed the percentage of total, large droplet, and small droplet steatosis in each case based on H&E slides. In all histology reviews, steatosis was assessed by visual estimate (i.e., unassisted by digital tools) and defined as the parenchymal area occupied by steatosis (numerator) over total liver parenchymal area (denominator).

Digital image analysis (DIA)

In each slide, three images were captured at ×100 magnification using Nikon DS-Fi2 digital microscope camera. Random images were taken if the steatosis was uniformly distributed throughout the slide. If the steatosis was heterogeneous, images representing the highest, intermediate, and lowest fat infiltration areas were obtained. The percent area of total steatosis (H&E and ORO slides) as well as large and small droplet steatosis were assessed using ImageJ image analysis software [12] (version 1.52a, National Institutes of Health, USA) and Nikon NIS-Elements BR4.30.02. Each image was sequentially analyzed three times by each software, and the average read was recorded as the final steatosis % value. Portal tracts, central veins, dilated sinusoids, and any areas of artifactual tissue defects were manually selected and excluded from the digital analysis (Supplementary Fig. 2 and Figs. 2, 3).

Biochemical triglyceride measurement

Fresh liver tissue was collected, immediately frozen on liquid nitrogen, and stored in −80 °C. Triglyceride measurements were performed on all samples. Briefly, triglyceride contents were determined in tissue lysates using a colorimetric assay and expressed as µg of lipid/mg of cellular protein. Mouse livers were homogenized and lysed in NETN buffer (20-mM Tris-HCl, pH 8.0; 100-mM NaCl; 1-mM EDTA; and 0.5% NP-40) supplemented with 5-mM NaF, 50-mM 2-glycerophosphate, and a protease inhibitor cocktail (Roche). Homogenates were incubated at 4 °C for 20 min under constant agitation, then centrifuged at 10,000 *g* for 10 min at 4 °C. Lipid content was measured by using the Infinity reagent (Thermo Fisher Scientific) according to the manufacturer's instructions [13].

Statistical analysis

Mouse and liver measurements were summarized with the median and interquartile range (IQR), and were compared

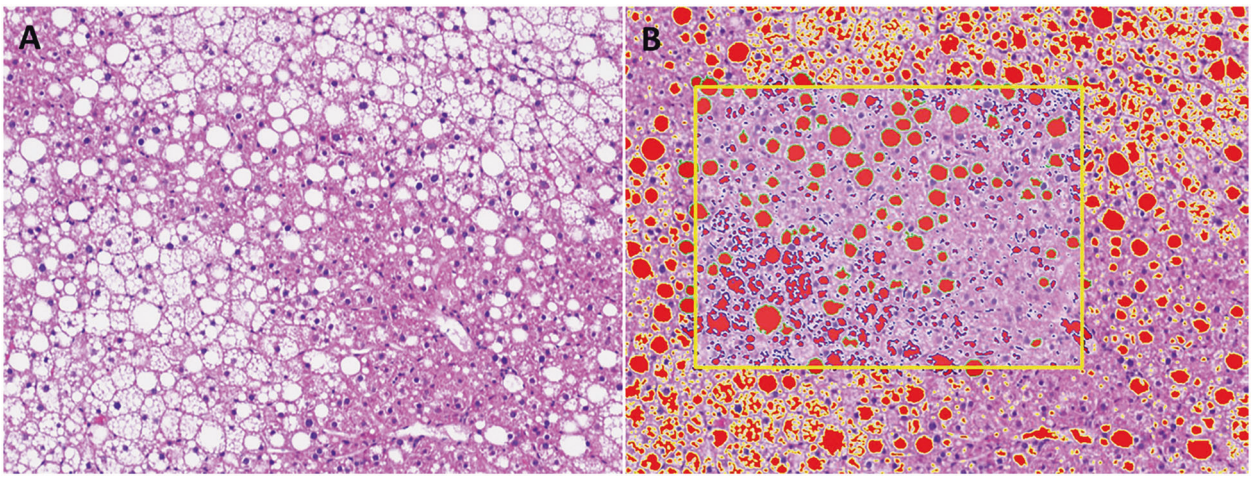

Fig. 2 Steatosis digital analysis. Steatosis (both large droplet and small droplet) on hematoxylin and eosin (H&E) slide (**A**). Large droplet steatosis digital image analysis of H&E slide (Nikon NIS-Elements BR4.30.02). Large droplet steatosis appears in red with a green rim within the yellow rectangular region of interest (**B**).

between the three groups (control, mild steatosis, moderate-to-severe steatosis) using pairwise Wilcoxon rank-sum tests. Correlations with the visual and digitally assessed steatosis percentages were estimated along with 95% confidence intervals using Fisher's z transformation. The reproducibility of the color space values from the spectrophotometer was assessed with intraclass correlation coefficients (ICCs). Comparisons of the color space axis values were performed between groups using mixed-effects linear regression models with a random intercept term to account for correlated observations within each mouse. To examine which color space axis value best discriminated between the moderate-to-severe steatosis mice versus the no-to-mild steatosis group, receiver operating characteristic analyses were conducted. The area under the curve (AUC) and cutoff that maximized the sensitivity (percentage of moderate-to-severe steatosis mice with a value ≥cutoff) and specificity (percentage of no-to-mild steatosis mice with a value <cutoff) were reported. A multivariate analysis was also performed to see how well a combination of the color space values would perform in discriminating between the mice groups. For this, considering each of the color space values, a logistic regression model was estimated using elastic net regularization with tenfold cross validation to select the largest value of the shrinkage parameter (lambda) that is within one standard error of the lambda that maximizes the cross-validated AUC. Multiple regression analysis was used to assess the predictive ability of spectrophotometric parameters for large droplet steatosis, including small droplet steatosis as an independent variable. Analyses were performed using SAS version 9.4, R version 3.6.2, and MedCalc® Software Version 19.15.

Results

Body weight and liver weight

As expected, body and liver weight were highest in the moderate-to-severe steatosis (median body weight 51.0 g, IQR: 48.8–53.3 g; median liver weight 2.8 g, IQR: 2.4–3.7 g), followed by the mild steatosis group (median body weight 41.5 g, IQR: 39.2–43.3 g; median liver weight 1.5 g, IQR: 1.3–1.7 g), then controls (median body weight 31.0, IQR: 29.7–32.9 g; median liver weight 1.5 g, IQR: 1.4–1.6 g). Body and liver weight for each group is presented in Supplementary Fig. 3.

Steatosis by H&E stain and visual assessment

All mice in the 8–20-week HFD group developed moderate-to-severe total (small + large droplet) steatosis (>30% and >60%, respectively) by H&E stain, as estimated by visual assessment. Among the group of mice on HFD for 2–4 weeks, 10 of 14 mice developed total steatosis in the mild range (1–30%) and were included in the study, while 4 of 14 mice had no steatosis and were excluded. The degree of steatosis (total, large droplet, and small droplet) in each group by visual estimate is shown in Fig. 4. None of the control mice developed steatosis. None of the mice in any of the groups had histologic evidence of significant inflammation, hepatocyte ballooning, Mallory hyaline, or fibrosis based on both H&E and trichrome stains.

Steatosis by DIA (H&E and ORO stains)

Visual estimation of total steatosis on H&E slides was very strongly correlated with DIA assessment of total steatosis

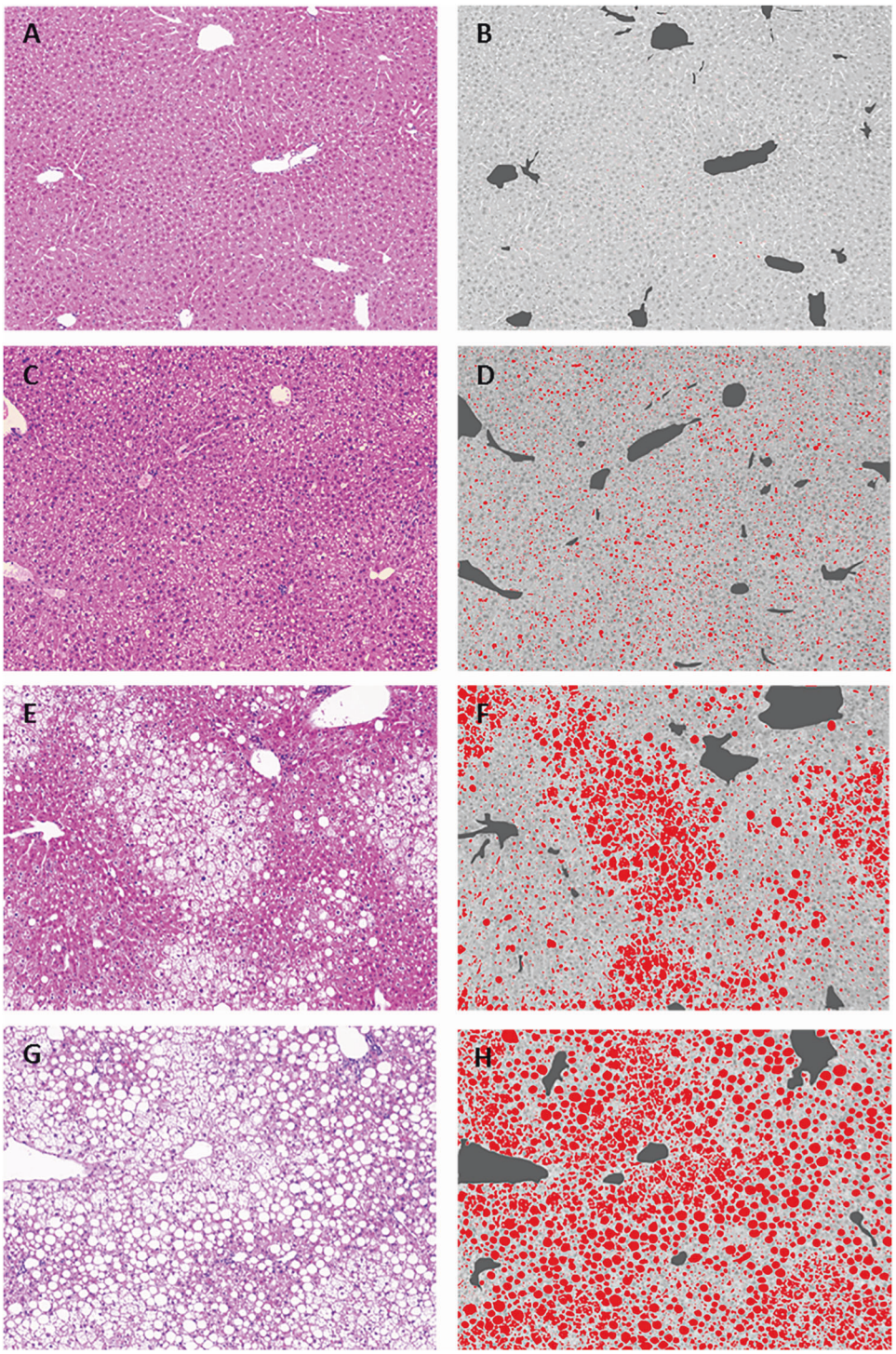

Fig. 3 Various degrees of steatosis and corresponding digital image analysis. A, **B** Normal control; **C**, **D** mild steatosis; **E**, **F** moderate steatosis; and **G**, **H** severe steatosis.

on H&E stains ($r = 0.94$, 95% CI 0.88–0.97), and with DIA of ORO stains ($r = 0.87$, 95% CI 0.74–0.94), but yielded significantly lower steatosis percentages (approximately half of the absolute percentage value obtained by visual assessment). Total steatosis DIA of H&E slides were also strongly correlated with DIA of ORO stains ($r = 0.90$, 95% CI 0.79–0.95). Estimation of large droplet steatosis by visual assessment showed moderate correlation with DIA estimation of large droplet steatosis ($r = 0.79$, 95% CI 0.60–0.89). Correlation values reflect statistical analysis of steatosis cases only. Results are shown in Fig. 5.

Tissue triglyceride quantitative analysis

Mice in the control group had median hepatic triglyceride levels of 50.6-μg/mg protein (IQR: 33.6–81.6), compared to

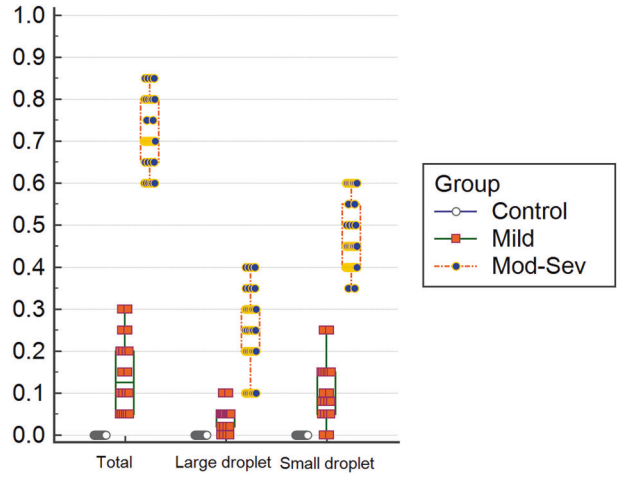

Fig. 4 Steatosis graph. Steatosis by visual estimation on H&E stain ($p < 0.001$ for all pairwise comparison among the three groups).

104.0-µg/mg protein (IQR: 94.8–132.2) in the mild steatosis group and 482.5-µg/mg protein (IQR: 312.6–684.0) in the moderate-to-severe steatosis group (Supplementary Fig. 4; $p < 0.001$ between all groups). There was strong correlation between triglyceride measurement and total steatosis by visual assessment of H&E slides ($r = 0.79$, 95% CI 0.65–0.88, $p < 0.0001$) by DIA of H&E slides ($r = 0.79$, 95% CI 0.64–0.87, $p < 0.0001$), and by DIA of ORO slides ($r = 0.79$, 95% CI 0.65–0.87, $p < 0.0001$) (Supplementary Fig. 5).

Spectrophotometry

The spectral reflectance graph of livers with various degrees of total steatosis was readily distinguishable from those of normal controls throughout nearly the entire visible spectrum, but especially beyond wavelengths of 450–500 nm, with differences becoming progressively more apparent into the green, yellow, and red ranges of visible light (Fig. 6).

Color coordinate values related to the "lightness" (black-white [L*] axis) and "yellowness" (yellow-blue [b*] axis) in the L*a*b* color space, all values in the tristimulus XYZ color space (Supplementary Fig. 6), as well as "c*" and "h*" in the L*c*h* color space were significantly different in the control, S1, and S2–3 groups. The median dominant wavelength was also significantly skewed toward the yellow range of the spectrum as steatosis increased between groups. The spectrophotometric values in the L*a*b*, XYZ, and L*c*h* color spaces and the calculated RBG and CMYK values for the three groups are presented in Table 1.

Most color space axis values showed very strong correlation with total steatosis by either visual estimate (H&E stains, r value of up to 0.91) or DIA (H&E and ORO stains, r value of up to 0.92), and strong correlation with biochemical quantitative tissue triglyceride measurement (r value of up to 0.79) (shown in Supplementary Table 1). The correlation between tissue triglycerides and total steatosis by H&E stain with visual assessment, H&E stain with DIA, and ORO stains with DIA was strong, with Pearson's coefficients of $r = 0.79$, $r = 0.78$, and $r = 0.79$, respectively.

Among the color space values in Table 2, when considered individually, the AUC was >0.90 for each color space value, indicating that any one of these values could discriminate well between the mice with moderate-to-severe vs. no-to-mild total steatosis. The AUC for a* (L*a*b* color space) performed the worst with AUC of 0.90; however, the AUC for each remaining value was ≥0.96, with % reflectance at wavelength 700 nm performing the best (AUC = 1 with 100% sensitivity and specificity at a cutoff of 45%). Using a cutoff of 45% reflectance, there was no overlap between no-to-mild steatosis (up to 30%) versus moderate-to-severe total steatosis (>30%) by visual assessment. These groups were also non-overlapping by DIA, although with lower absolute numbers for steatosis percentage (Fig. 7). The remaining spectrophotometric parameters were also useful but had a higher degree of overlap between all groups. A multivariate analysis was also performed to see how a combination of the color space values would perform in discriminating between the different degrees of steatosis (see "Materials and methods"). A logistic regression model that includes a* (from L*a*b* color space) along with the % reflectance at 430 and 700 nm performed perfectly with AUC of 1. Given that a simple cutoff for a single parameter is simpler to implement and performs equally well (rather than a more complicated equation), we felt that the more complex approach was not necessary.

On multiple regression analysis that included individual spectrophotometric parameters and small droplet steatosis as independent variables in the model, the percent large droplet steatosis, as evaluated by H&E stain with visual assessment, was independently predicted by L*, X, Y, and % reflectance at wavelengths of 490–700 nm ($p < 0.05$), with the most significant predictor being % reflectance at wavelength 700 nm. Spectrophotometry-derived parameters performed better at predicting large droplet steatosis on H&E stains assessed by DIA, with L*, b*, X, Y, Z, h*, R, G, B, C, M, Y, K, and wavelengths 400–700 nm being independent predictors ($p < 0.05$) in models that included small droplet steatosis. Percent reflectance at wavelength 700 nm was again the most significant independent predictor. We did not evaluate small and large droplet fractions on ORO stains due to the fact that this method is not suitable for this analysis. Finally, the color space values and spectral reflectance percentages were highly reproducible across both observations within each mouse liver, with ICCs all above 0.97.

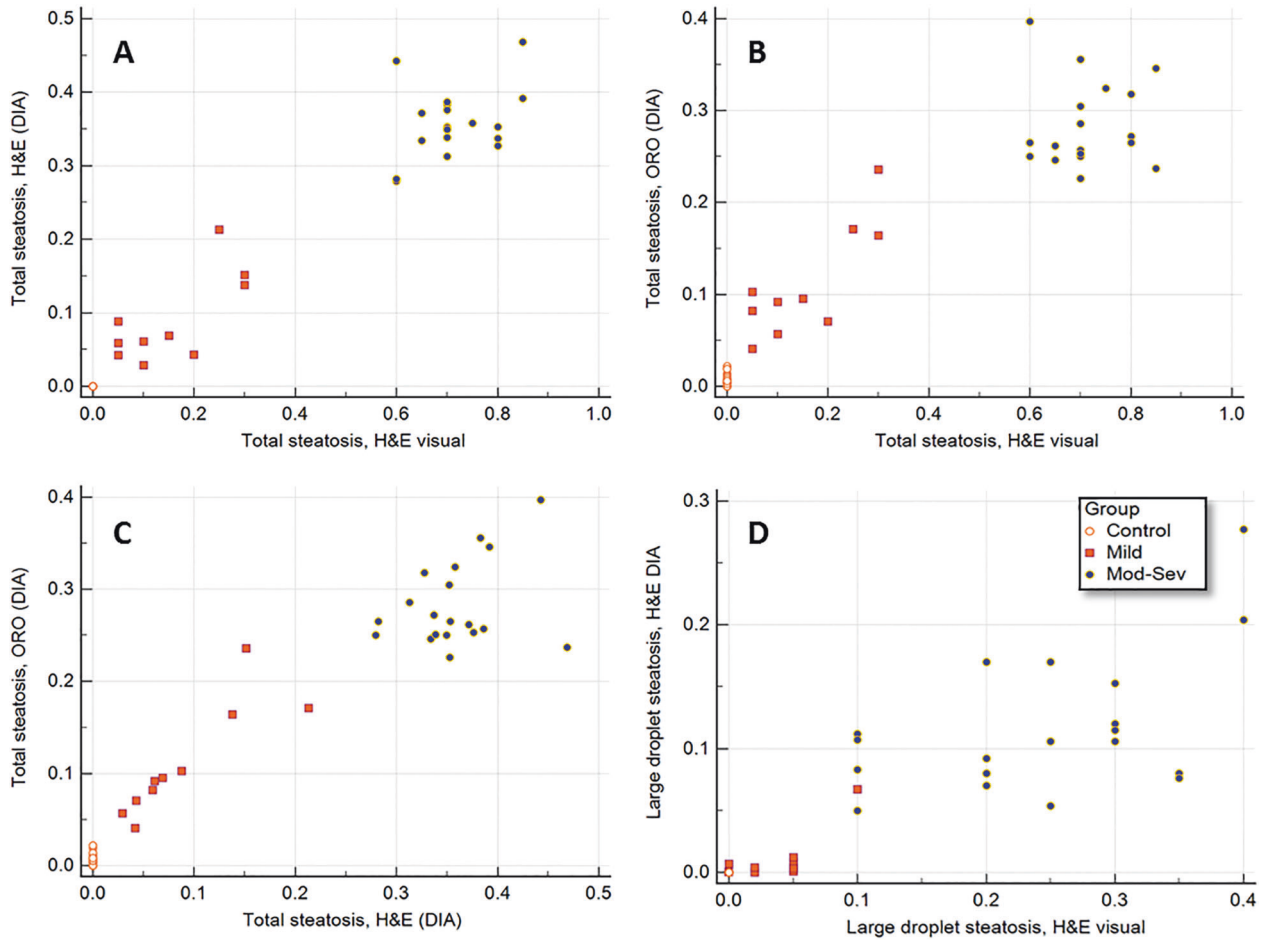

Fig. 5 Steatosis assessment by different methods and their correlation with one another. A Visual estimation of total steatosis on hematoxylin and eosin (H&E) stain in correlation with digital image analysis (DIA) of H&E slides ($r = 0.94$); **B** Visual estimation of total steatosis on H&E slides in correlation with DIA of oil-red-O (ORO) stains ($r = 0.87$); **C** DIA of total steatosis on H&E slides in correlation with DIA of ORO stains ($r = 0.90$); **D** Visual estimation of large droplet steatosis on H&E stains in correlation with large droplet steatosis assessment by DIA ($r = 0.79$).

Discussion

Histopathologic assessment of steatosis by histochemical techniques (H&E frozen section with or without fat stains and "visual" steatosis estimation by a pathologist) is still the most commonly utilized method for steatosis assessment during organ procurement, as risk stratification for graft outcomes has largely been derived from studies based on this practice. However, novel methods for the pretransplant evaluation of steatosis in cadaveric donors could potentially be useful for several reasons. While experienced surgeons may be able to visually identify steatosis falling in the extremes of the spectrum, estimating steatosis percentage by "naked eye" inspection of the potential allograft is significantly more challenging in cases showing fatty change in the mild-to-moderate range [14], in which precise quantitation is still crucial for decision-making purposes. In addition, immediate availability of routine pathologic examination of a potential donor biopsy by experienced pathologists varies in different centers. Even after biopsy results are obtained, the surgeon still needs to deal with uncertainties stemming from the lack of standardization and subjectivity of the pathologic quantitation of steatosis. The "visual" method of pathologic evaluation—whereby H&E slides with or without fat stains such as Sudan IV or ORO are subjectively assessed for percentage of tissue fat—is currently the standard of care in most transplant centers, in spite of a number of studies demonstrating its limitations [15–17]. Many factors contribute to the shortcomings of this method, including the intrinsic difficulty and subjectiveness of quantifying percentages in surface areas without the aid of computerized analytical tools as well as the variability in histologic sectioning and staining quality in different laboratories. In addition, quantitative or semiquantitative evaluation of steatosis in donor biopsies is compounded by the fact that results rely on the interpretation of frozen sections, which introduce important additional challenges compared to routine histologic slides (using formalin-fixed,

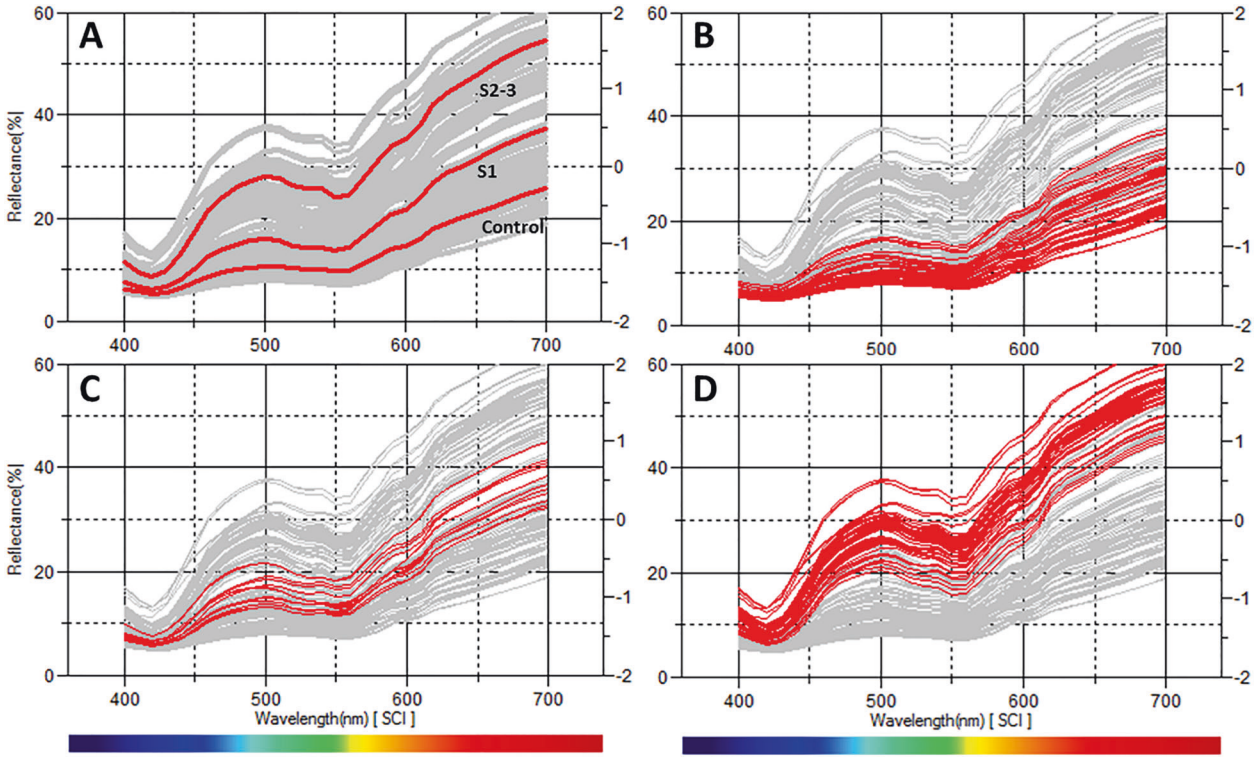

Fig. 6 Spectral reflectance graphs. A Average spectral reflectance for controls, mild steatosis (S1), and moderate-to-severe steatosis (S2–3); spectral reflectance curves for individual measurements in the control (**B**), S1 (**C**), and S2–3 (**D**) groups.

Table 1 Spectrophotometric values for different color spaces (CIE L*a*b*, XYZ, L*c*h*), dominant wavelength (nm), and % reflectance at 700 nm in the different steatosis groups.

Color space axis	Control	S1	S2–3	*p* value
L*	39.8 (36.9–42.9)	47.4 (45.6–50.5)	61.0 (58.8–62.4)	<0.001
b*	12.2 (11.0–13.8)	16.0 (14.8–16.9)	19.9 (19.2–20.7)	<0.001
X	11.5 (10.0–13.6)	17.1 (16.0–19.6)	29.4 (27.3–30.8)	<0.001
Y	11.1 (9.5–13.1)	16.3 (15.0–18.8)	29.3 (26.8–30.9)	<0.001
Z	7.9 (7.1–9.1)	10.8 (10.1–12.4)	19.3 (17.4–20.6)	<0.001[a]
c*	14.9 (13.5–15.9)	18.6 (17.6–19.7)	20.9 (20.1–21.9)	<0.001
R	113.5 (107–123)	137 (134–146)	170.5 (167–174)	<0.001
B	74 (71–79)	86 (83–92)	112 (106–117)	<0.001
G	89 (82–96)	106.5 (102–114)	142 (136–146)	<0.001
C	47 (45–49)	41 (38–42)	33 (32–34)	<0.001
M	58 (56–60)	54 (51–56)	41 (40–44)	<0.001
Y	66 (64–67)	65 (64–66)	59 (57–62)	<0.001[b]
K	29 (25–34)	19 (15–21)	4.5 (3–6)	<0.001[a]
h*	57.6 (53.3–60.5)	60.0 (56.9–62.4)	72.0 (69.9–73.0)	<0.001[b]
Dominant wavelength	582.5 (581.3–584.1)	581.7 (580.6–583.2)	577.3 (576.9–578.1)	<0.001[b]
% reflectance at 700 nm	24.4 (22.1–28.9)	36.3 (33.7–40.7)	55.2 (52.7–56.9)	<0.001

Values are expressed as median (interquartile range). All *p* values were calculated using mixed-effects linear regression.

[a]$p = 0.002$ for control vs. S1 and <0.001 for S2–3 against either control or S1.

[b]$p > 0.05$ for control vs. S1 and <0.001 for S2–3 against either control or S1.

paraffin-embedded tissue). These are collectively referred to as "frozen section artifacts," whereby various freezing-related changes result in overall poor quality of slides when compared to routine H&E sections. Among frozen section artifacts, the most significant in this context is the ubiquitous presence of cytoplasmic vacuolization of hepatocytes

Table 2 Correlation (95% confidence interval) between color space axis values and total steatosis assessed by visual estimate (hematoxylin and eosin), digital image analysis (DIA) (hematoxylin and eosin), and biochemical quantitative tissue triglyceride measurement (μg/mg protein).

Color space axis	Steatosis, visual (H&E)	Steatosis, DIA (H&E)	Steatosis, DIA (ORO)	Tissue triglyceride
L*	$r = 0.90$ (0.85–0.93)	$r = 0.91$ (0.86–0.94)	$r = 0.91$ (0.86–0.95)	$r = 0.78$ (0.63–0.87)
b*	$r = 0.86$ (0.80–0.91)	$r = 0.87$ (0.80–0.91)	$r = 0.88$ (0.79–0.93)	$r = 0.69$ (0.50–0.81)
X	$r = 0.90$ (0.85–0.93)	$r = 0.91$ (0.86–0.94)	$r = 0.92$ (0.86–0.95)	$r = 0.79$ (0.65–0.88)
Y	$r = 0.90$ (0.85–0.93)	$r = 0.91$ (0.86–0.94)	$r = 0.92$ (0.86–0.95)	$r = 0.79$ (0.65–0.88)
Z	$r = 0.88$ (0.82–0.92)	$r = 0.89$ (0.83–0.92)	$r = 0.89$ (0.82–0.94)	$r = 0.79$ (0.64–0.87)
c*	$r = 0.82$ (0.74–0.88)	$r = 0.82$ (0.74–0.88)	$r = 0.83$ (0.72–0.90)	$r = 0.65$ (0.44–0.78)
R	$r = 0.90$ (0.85–0.93)	$r = 0.90$ (0.86–0.93)	$r = 0.91$ (0.85–0.95)	$r = 0.77$ (0.62–0.86)
G	$r = 0.90$ (0.85–0.93)	$r = 0.91$ (0.86–0.94)	$r = 0.92$ (0.86–0.95)	$r = 0.78$ (0.64–0.87)
B	$r = 0.88$ (0.83–0.92)	$r = 0.89$ (0.84–0.93)	$r = 0.90$ (0.82–0.94)	$r = 0.78$ (0.63–0.87)
C	$r = -0.89$ (−0.93 to −0.84)	$r = -0.90$ (−0.93 to −0.85)	$r = -0.91$ (−0.95 to −0.85)	$r = -0.77$ (−0.87 to −0.62)
M	$r = -0.90$ (−0.93 to −0.85)	$r = -0.90$ (−0.93 to −0.86)	$r = -0.91$ (−0.95 to −0.86)	$r = -0.79$ (−0.87 to −0.65)
Y	$r = -0.75$ (−0.82 to −0.64)	$r = -0.76$ (−0.83 to −0.66)	$r = -0.75$ (−0.85 to −0.60)	$r = -0.71$ (−0.82 to −0.52)
K	$r = -0.81$ (−0.87 to −0.73)	$r = -0.83$ (−0.88 to −0.75)	$r = -0.78$ (−0.87 to −0.64)	$r = -0.65$ (−0.79 to −0.44)
h*	$r = 0.85$ (0.78–0.90)	$r = 0.85$ (0.78–0.90)	$r = 0.86$ (0.77–0.92)	$r = 0.71$ (0.53–0.83)
% Reflectance at 700 nm	$r = 0.91$ (0.88–0.94)	$r = 0.92$ (0.88–0.95)	$r = 0.92$ (0.87–0.95)	$r = 0.78$ (0.63–0.87)

H&E hematoxylin and eosin, *r* Pearson correlation coefficient.

[18], which cannot reliably be distinguished from microvesicular or small droplet steatosis, rendering evaluation of the latter extremely difficult. Finally, organ procurement often takes place at hospitals, which are remote from the transplant center and may require on-site histologic assessment of the liver at institutions where the availability of experienced pathologists may be limited, especially after-hours when organ procurement usually occurs.

In view of the limitations of the currently employed methods, we sought to evaluate spectrophotometry, a technique widely utilized and generally recognized as the gold standard in color assessment, quality control, and color communication by various industries, as an alternative approach to the quantification of hepatic steatosis, in comparison with various methods steatosis analysis. This technique has been shown to be useful in the evaluation of the age of skin bruises in forensic medicine [19] and has been employed successfully in the practice of dermatology, including in the evaluation of skin type/pigmentation and monitoring of certain diseases such as acanthosis nigricans and psoriasis [6, 7, 11]. Therefore, we believe that this method also has the potential to serve a very useful tool in the evaluation of hepatic steatosis in the setting of organ procurement.

In this study, we evaluated the accuracy of spectrophotometry in the visible light spectrum for the assessment of steatosis. The main advantages of this technique stem from the wide commercial availability of instruments at a relatively affordable cost, user-friendly operation, ability to provide immediate results (and potential use as point-of-care instrument), and the existence of a worldwide industry dedicated to color sensing and communication, which already utilizes highly standardized equipment and color analysis tools. Therefore, this represents a tool that could be adopted without incurring prohibitive costs, requiring extensive training, or specialized skills.

We showed that even relatively subtle variations in the liver surface color due to increased lipid content can readily be detected spectrophotometrically, and numerous parameters included in various color spaces can fairly reliably distinguish steatosis of various degrees, as assessed by the different methods we have utilized. Several of spectrophotometric parameters we studied were shown to be highly predictive of total steatosis, with AUC of 0.90 or above for all color spaces. % reflectance at 700 nm had the best performance, showing no overlap between the 0 and 30% steatosis versus >30% steatosis study groups.

A subset of these parameters, especially by DIA, was also predictive of large droplet steatosis independently from small droplet steatosis—a finding which would have obvious relevance for the application of this technique in the setting of liver allograft procurement. Although the precise biophysical basis for this distinction is not completely understood, as previously noted by Graaf et al. [20] and Evers et al. [21], there is evidence to suggest that scattering parameters in different wavelengths is dependent on particle size. Hence, small and large droplet steatosis may indeed have different spectrophotometric signatures.

To our knowledge, our study was the first to utilize the concept of color spaces in the setting of steatosis. Briefly,

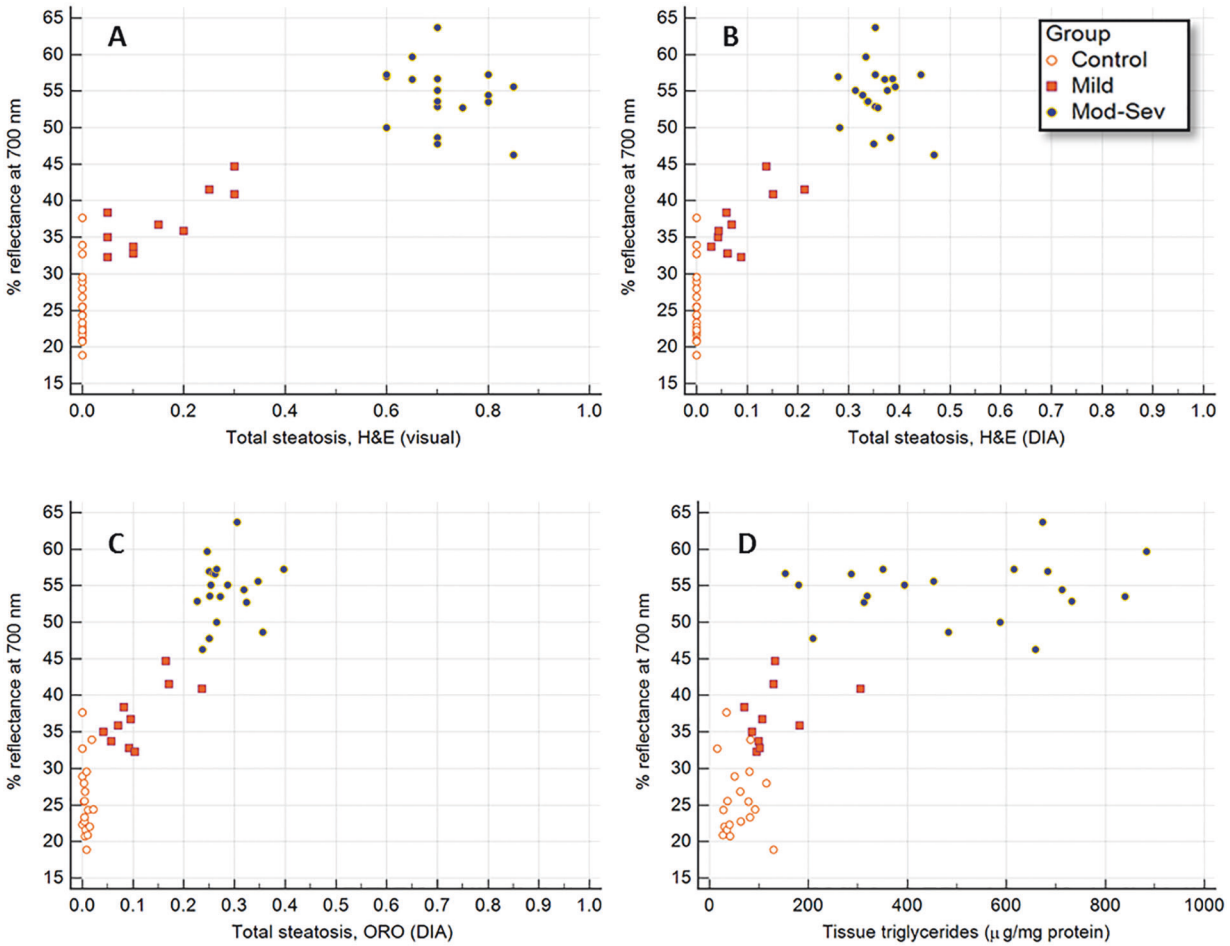

Fig. 7 Correlation between % spectral reflectance at wavelength 700 nm by surface spectrophotometry and degree of histologic steatosis, as measured by different methods. A Visual assessment of hematoxylin and eosin (H&E) slides ($r = 0.91$, $p < 0.0001$); **B** digital image analysis (DIA) of H&E slides ($r = 0.92$, $p < 0.0001$); and **C** DIA of oil-red-O stains ($r = 0.92$, $p < 0.0001$). Correlation between % spectral reflectance at wavelength 700 nm and tissue triglycerides ($r = 0.77$, $p < 0.0001$) (**D**).

the concept of color space refers to a system that expresses a range of colors in numbers (coordinates), forming a three-dimensional object containing all realizable combinations, each representing a specific color. Each axis of this three-dimensional color space represents a defining aspect of color, such as lightness, saturation, or hue, etc., depending on the specific system. Common color spaces utilized in color communication include L*a*b* (in which L* indicates the "lightness" of the color while a* and b* indicate chromacity coordinates in the green-red and blue-yellow axis, respectively), L*c*h (where L* also indicates "lightness", c* chromacity, and h* hue angle), and XYZ (or "tristimulus" value based on the three-component theory of human color vison). While these parameters are mathematically derived from the measured spectral reflectance data within the visible light spectrum, they represent an objective and highly standardized way to precisely describe and communicate colors (as a three-number coordinate), therefore being potentially useful in the context of both research and clinical practice.

McLaughlin et al. [22] and Westerkamp et al. [23] first described the potential utility of reflectance spectroscopy (in the near-infrared wavelength range, from 1000 to 1600 nm) in the setting of fatty liver disease and were able to demonstrate the accuracy of this technique in the distinction of normal livers, mild steatosis, and moderate–severe steatosis. A similar technique was also studied using in vivo percutaneous instruments in rats (single fiber spectroscopy) [24] and in humans (diffuse reflectance spectroscopy [DRS] through optical fiber) [25] and proved useful in the distinction between different degrees of steatosis. Using an optical needle and DRS, Evers et al. [21] have also reported progressively higher light absorption in the vicinity of the 1200-nm wavelength region (within the near-infrared range) with increasing degrees of steatosis in humans—with a strong correlation between fat fraction % by DRS and pathologic readings ($r = 0.85$) in vivo. These studies,

however, utilized either customized equipment or tools that are costly or not widely available. In addition, none of these studies described techniques that were able to specifically correlate with large droplet steatosis.

In contrast to previous studies, we have utilized flushed liver tissue (with standard preservation solution) in order to more closely simulate the conditions seen during human organ procurement. Non-flushed livers (both murine and human) often show a highly variegated surface due to uneven blood distribution, clotting, tissue hypoxia, among other factors. Organ flushing eliminates or significantly decreases tissue color variegation and also diminishes the concentration of various blood lipids as well as pigments such as hemoglobin and bilirubin, which are known to interfere with—or at least be detected by—spectral readings [26, 27]. Of these, hemoglobin would likely represent the most relevant chromophore in this setting given its abundance within the highly vascularized liver tissue and high degree of reflectance in the 600–700-nm wavelength of the visible spectrum [28].

One of the challenges of studying a new technique for steatosis assessment is the fact that our current gold standard (i.e., histopathologic assessment) is known to have significant limitations. To minimize misinterpretations related to an imperfect gold standard, we used different methods of assessment, including visual, digital analysis of both H&E stains and ORO stains, as well as tissue biochemical measurements. Also, our mouse model developed a significant component of small droplet steatosis (a common feature of several animal models of steatosis, especially HFD), in contrast to what is typically seen in human fatty liver disease, in which large droplet steatosis usually predominates. We have, nonetheless, opted to utilize a HFD murine model in this study—rather than other available models such as methionine/choline deficiency, choline deficiency-HFD, and hepatocyte-specific PTEN deficiency mice—due to the presence of no more than minimal inflammation and relatively late development of fibrosis, factors that could potentially represent confounding variables for spectrophotometric evaluation.

Although we have demonstrated that spectrophotometric analysis of the visible light spectrum is strongly correlated with steatosis in a mouse model, further studies are needed to establish with certainty whether this technique, as applied here, would also be accurate in the evaluation of human liver allografts. In addition, although steatosis assessment is essential in the setting of liver allograft procurement, other histopathologic features such as inflammation and fibrosis are also relevant. It is unclear, however, whether the later abnormalities are detectable by visible light spectrophotometry, or whether they would interfere with steatosis assessment to any meaningful extent.

In summary, we have demonstrated in this study that surface spectrophotometry represents an accurate technique for assessment of steatosis (including large droplet steatosis, specifically) in mice that correlates well with steatosis measurement by various currently available tissue-based methods, including biochemical quantitative analysis and detailed histopathologic assessment using digital pathology. The application of color space coordinates in this setting is a novel tool that can be useful for both clinical and research purposes. Visible light-spectrum surface spectrophotometry, as described here, represents a very promising tool to be utilized in liver allograft procurement, but further studies are necessary for validation of this technique in humans.

Data availability

All data collected and analyzed in this study are available.

Author contributions All authors contributed to the conception and design, data acquisition, analysis, and/or interpretation of the data, critical revision for important intellectual content, and gave final approval of the version to be published.

Funding Funding for this study has been provided by Mayo Clinic Department of Laboratory Medicine and Pathology (intra-departmental funding).

Compliance with ethical standards

Conflict of interest The authors declare no competing interests.

Ethics approval All protocols and procedures were approved by our hospital's Institutional Animal Care and Use Committee (IACUC), and studies were conducted in adherence to the NIH Guide for the Care and Use of Laboratory Animals.

Publisher's note Springer Nature remains neutral with regard to jurisdictional claims in published maps and institutional affiliations.

References

1. Linares I, Hamar M, Selzner N, Selzner M. Steatosis in liver transplantation: current limitations and future strategies. Transplantation. 2019;103:78–90.
2. Chu MJ, Dare AJ, Phillips AR, Bartlett AS. Donor hepatic steatosis and outcome after liver transplantation: a systematic review. J Gastrointest Surg. 2015;19:1713–24.
3. He WH, Park CJ, Byun S, Tan D, Lin CY, Chee W. Evaluating the relationship between tooth color and enamel thickness, using twin flash photography, cross-polarization photography, and spectrophotometer. J Esthet Restor Dent. 2020;32:91–101.
4. Paul S, Peter A, Pietrobon N, Hammerle CH. Visual and spectrophotometric shade analysis of human teeth. J Dent Res. 2002;81:578–82.
5. He HJ, Wu D, Sun DW. Nondestructive spectroscopic and imaging techniques for quality evaluation and assessment of fish and fish products. Crit Rev Food Sci Nutr. 2015;55:864–86.
6. Pershing LK, Tirumala VP, Nelson JL, Corlett JL, Lin AG, Meyer LJ, et al. Reflectance spectrophotometer: the dermatologists'

sphygmomanometer for skin phototyping? J Invest Dermatol. 2008;128:1633–40.
7. Devpura S, Pattamadilok B, Syed ZU, Vemulapalli P, Henderson M, Rehse SJ, et al. Critical comparison of diffuse reflectance spectroscopy and colorimetry as dermatological diagnostic tools for acanthosis nigricans: a chemometric approach. Biomed Opt Express. 2011;2:1664–73.
8. Devpura S, Barton KN, Brown SL, Palyvoda O, Kalkanis S, Naik VM, et al. Vision 20/20: the role of Raman spectroscopy in early stage cancer detection and feasibility for application in radiation therapy response assessment. Med Phys. 2014;41:050901.
9. Hughes VK, Langlois NE. Visual and spectrophotometric observations related to histology in a small sample of bruises from cadavers. Forensic Sci Med Pathol. 2011;7:253–6.
10. Petzold A, Keir G, Sharpe TL. Why human color vision cannot reliably detect cerebrospinal fluid xanthochromia. Stroke. 2005;36:1295–7.
11. Tzeng SY, Guo JY, Yang CC, Hsu CK, Huang HJ, Chou SJ, et al. Portable handheld diffuse reflectance spectroscopy system for clinical evaluation of skin: a pilot study in psoriasis patients. Biomed Opt Express. 2016;7:616–28.
12. Schneider CA, Rasband WS, Eliceiri KW. NIH Image to ImageJ: 25 years of image analysis. Nat Methods. 2012;9:671–5.
13. Zang M, Zuccollo A, Hou X, Nagata D, Walsh K, Herscovitz H, Brecher P, Ruderman NB, Cohen RA. AMP-activated protein kinase is required for the lipid-lowering effect of metformin in insulin-resistant human HepG2 cells. J Biol Chem. 2004;279:47898–905.
14. Imber C. Hepatic steatosis and its relationship to transplantation. Liver Transplant. 2002;8:415–23.
15. Marsman H, Matsushita T, Dierkhising R, Kremers W, Rosen C, Burgart L, et al. Assessment of donor liver steatosis: pathologist or automated software? Hum Pathol. 2004;35:430–5.
16. El-Badry AM, Breitenstein S, Jochum W, Washington K, Paradis V, Rubbia-Brandt L, et al. Assessment of hepatic steatosis by expert pathologists: the end of a gold standard. Ann Surg. 2009;250:691–7.
17. Le Naour F, Gadea L, Danulot M, Yousef I, Vibert E, Wavelet M, et al. Quantitative assessment of liver steatosis on tissue section using infrared spectroscopy. Gastroenterology. 2015;148:295–7.
18. Brunt EM. Surgical assessment of significant steatosis in donor livers: the beginning of the end for frozen-section analysis? Liver Transpl. 2013;19:360–1.
19. Yajima Y, Funayama M. Spectrophotometric and tristimulus analysis of the colors of subcutaneous bleeding in living persons. Forensic Sci Int. 2006;156:131–7.
20. Graaff R, Aarnoudse JG, Zijp JR, Sloot PMA, Demul FFM, Greve J, et al. Reduced light-scattering properties for mixtures of spherical-particles—a simple approximation derived from Mie calculations. Appl Optics. 1992;31:1370–6.
21. Evers DJ, Westerkamp AC, Spliethoff JW, Pully VV, Hompes D, Hendriks BH, et al. Diffuse reflectance spectroscopy: toward real-time quantification of steatosis in liver. Transpl Int. 2015;28:465–74.
22. McLaughlin BL, Wells AC, Virtue S, Vidal-Puig A, Wilkinson TD, Watson CJ, et al. Electrical and optical spectroscopy for quantitative screening of hepatic steatosis in donor livers. Phys Med Biol. 2010;55:6867–79.
23. Westerkamp AC, Pully VV, Karimian G, Bomfati F, Veldhuis ZJ, Wiersema-Buist J, et al. Diffuse reflectance spectroscopy accurately quantifies various degrees of liver steatosis in murine models of fatty liver disease. J Transl Med. 2015;13:309.
24. Piao D, Sultana N, Holyoak GR, Ritchey JW, Wall CR, Murray JK, et al. In vivo assessment of diet-induced rat hepatic steatosis development by percutaneous single-fiber spectroscopy detects scattering spectral changes due to fatty infiltration. J Biomed Opt. 2015;20:117002.
25. Reistad N, Nilsson JH, Bergenfeldt M, Rissler P, Sturesson C. Intraoperative liver steatosis characterization using diffuse reflectance spectroscopy. HPB. 2019;21:175–80.
26. Xu JL, Riccioli C, Sun DW. An overview on nondestructive spectroscopic techniques for lipid and lipid oxidation analysis in fish and fish products. Compr Rev Food Sci Food Saf. 2015;14:466–77.
27. Hernandez B, Saenz C, Alberdi C, Dineiro JM. CIELAB color coordinates versus relative proportions of myoglobin redox forms in the description of fresh meat appearance. J Food Sci Technol. 2016;53:4159–67.
28. Can OM, Ulgen Y. Estimation of free hemoglobin concentrations in blood bags by diffuse reflectance spectroscopy. J Biomed Opt. 2018;23:1–12.